CHAPTER 4

Nitrogen/sulfur-co-doped carbon quantum dots: a biocompatible material for the selective detection of picric acid in aqueous solution and living cells

4.1. Introduction

During the past decades, carbon quantum dots (CQDs) act as an attractive class of bright fluorescent carbon-based nano-materials having a size less than 10 nm. They have several versatile properties such as large surface area, good photostability, low-toxicity, tunable excitation wavelength, high water solubility, optical charge transfer, and eco-friendly. Considering these properties, they have been utilized extensively in several fields such as sensing, photodynamic therapy, drug delivery, food industry, bio-imaging, LED's devices, catalysis, and wastewater treatment. [SG Liu *et al.* (2018), J Li *et al.* (2018), Q Ye *et al.* (2016), L Hu *et al.* (2017), X Jiang *et al.* (2019)] Several experimental strategies for the development of CQDs evolved counting arc discharge, [J Xu *et al*. (2011)] laser ablation, [H Li *et al.* (2010)] microwave irradiation, [F Wang *et al.* (2010)] electrochemical oxidation, [J Zhou *et al*. (2010)] chemical oxidation, [F Yang *et al.* (2012)] and hydrothermal treatment.[ZC Yang *et al.* (2011)] Among them, the hydrothermal technique is used preferably because of its simplicity, excellent response, and environmental friendliness. In recent years, many research efforts are focusing on the CQDs synthesis, which undergoes fundamental techniques such as surface functionalization and doping with different hetero-atoms to enhance the optical properties. [TK Mondal *et al.* (2018)]

2, 4, 6-trinitrophenol is the most hazardous nitro-containing aromatic organic compound. [Y Wan *et al.* (2019)] It is also known as picric acid (PA). Recently, PA has attracted considerable research attention due to the more explosive ability and extensive uses in several fields such as dye industry, pesticides, pharmaceuticals, rocket fuel, fireworks, explosive materials, pigments, and medicine. [S Liu *et al*. (2018), X Deng *et al.* (2015), BB Chen *et al*. (2016), B Wang *et al*. (2017), ZM Khan *et al.* (2020)] The minimum

concentration of PA can contaminate the surrounding environments, soils, and aqueous water, which give rise to numerous diseases for a human being such as cancer, anemia, cyanosis, respiratory problems, and central nervous system. [M Rong *et al.* (2015), M Wang *et al.* (2019), M Tian *et al.* (2018), Y Wang *et al.* (2018)] Consequently, it is an interesting task to expand a facile, rapid, and highly selective analytical technique for the detection of nitro-explosives in aqueous solution and biological system.

Numerous conventional strategies have been carried out for the testing of explosives such as mass spectroscopy, [L Barron *et al.* (2014)] Infrared and Raman spectroscopy, [P Srinivasan *et al.* (2006)] Surface-enhanced Raman scattering (SERS), [H Ko *et al.* (2009)] electrochemical methods, [Ho MY *et al.* (2012)] High-Performance Liquid Chromatography (HPLC) [S Babaee *et al.* (2010), AB Siddique *et al.* (2018)] and colorimetric. [Y Peng *et al.* (2011)] Nonetheless, these techniques have many difficulties, such as highly sophisticated, time-consuming, bound their prevalent use and expensive instruments. Recently, a fluorescence-based method has become an alternative detection technique for the nitro-explosives because of its excessive sensitivity and fast reaction time.

However, various fluorescent probes, including metal nano-particle, [M Hussain *et al.* (2016)] metal-organic frameworks, [X Zhang *et al.* (2019)] fluorescence dyes, [X Lu *et al.* (2019)] carbon nano-sheets, [C Zhang *et al.* (2017)] , and semiconductor quantum dots [A Pal *et al*. (2016)] have been prepared for the sensing of nitro explosives. Previously, many research co-workers have reported the sensitive and selective fluorescence probe for the testing of picric acid. Such as, Vandana *et al*. described the selective detection of PA by hexaphenylbenzene derivative. [S Pramanik *et al.* (2013)] Meng *et al*. have synthesized organic polymer nanotubes as bifunctional materials for the selective detection of Picric acid.

[M Wang *et al*. (2018)] Jian *et al.* reported fluorescent Ag nanoclusters for the selective sensing of PA. [JR Zhang *et al.* (2016)] Bingxin Liu *et al.* have reported polymer nano-material CdTe/ZnS quantum dots for the determination of PA. [B Liu *et al.* (2014)] Xue-Gang *et al.* have designed Iridium (III) nano-aggregates for the detection of PA [X-G Hou *et al.* (2014)] However, most of these synthesized materials involved the hazardous dye, toxic metals, and expensive reagent, which showed the harmful effect on the human beings and environmental friendliness. [Zhao Z *et al.* (2016)] In latest years, fluorescence-based sensors in particularly doped carbon quantum dots [C Han *et al.* (2016)] (without hazardous metals) have been attracted numerous advantages along with excessive sensitivity, less time consuming, low price, good selectivity, and accuracy for the detection of PA in aqueous samples.

In this work, we have synthesized water-soluble fluorescent carbon quantum dots with strong blue luminescence along with high QY of 37.8% through one-pot hydrothermal treatment using CA and TSC as the reaction source. The doped NS-CQDs by this method emitted blue fluorescence at 365 nm excitation wavelength under the UV-light. The as-organized NS-CQDs was characterized thoroughly by using various advanced techniques, namely XRD, TEM, IR, DLS, XPS, UV, and Fluorescence spectrophotometer analysis. Interestingly, the as-prepared NS-CQDs can perform as an effectual fluorescent-based nano-probe for selective sensing of PA in the buffer as well as in living cells and aqueous solution.

4.2. Materials and method

4.2.1. Synthesis of NS-CQDs

The NS-CQDs were prepared by the facile one-pot hydrothermal method. Thoroughly, CA (2 g) and TSC (1 g) were mixed into the 150 mL of ultrapure water. At that

time, the prepared solution was transported into the stainless steel Teflon-lined autoclave (250 mL) and heated at 180 ^{o}C for 5 h. Subsequently, the autoclave was cooled at room temperature (RT), and the obtained light brown solution was centrifuged at 15,000 rpm for 30 minutes to remove the foreign and agglomerated particles. The supernatant part was taken and purified through the 0.22 μm syringe filter. After that, the purified NS-CQDs solution was reserved at 4 ^{o}C for more reports and sensing applications.

4.2.2. Assay for the detection of PA

At RT, the 50 μL NS-CQDs were maintained in the 2 mL of sodium acetate (Na-Ac) buffer (0.2 M, pH 2). The prepared different concentration of PA solution was added into the NS-CQDs solution and shaken gently for 15 sec. The obtained mix solution was transposed into the 3 mL of fluorescence cuvette, and emission intensities were recorded with the excitation of 360 nm using a fluorescence spectrophotometer.

Further, the limit of the detection was determined by the equation signal-to-noise ratio 3 given in chapter 2 (equation 2.2)

Meanwhile, the Stern-Volmer quenching constant was determined from the equation 2.3 given in chapter 2.

4.2.3 Cell Culture

Cervical cancer cell line HeLa was cultured in Dulbecco's Modified Eagle Medium (Gibco) supplemented with 10% Fetal Bovine Serum (Gibco), Penicillin and Streptomycin (Invitrogen) maintained at 5% CO_2 in a humidified incubator at 37^{0}C.

4.2.4 Cytotoxicity study of NS-CQDs

The cells were first treated with increasing concentrations of NS-CQDs for 15 minutes and subjected to MTT assay as per standard protocol. Absorbance was taken at 540 nm in the Synergy H1 microplate reader (version 2.09.1) and represented with the help of Prism 5.0.

4.2.5. Quantification of cellular fluorescence

Determination of the least concentration of NS-CQDs apt for imparting fluorescence was accomplished with pre-treatment of the cells with NS-CQDs with concentration ranging from 1 to 10 mg/ml for 15 minutes, prior to estimation of cellular fluorescence intensity in a microplate reader (Synergy H1 version 2.09.1).

The sensitivity of the NS-CQDs to intracellular PA was tested by exposing the cells to 8 mg/ml NS-CQDs for 15 minutes, followed by treatment with variable levels of PA. The retention of fluorescence was immediately acquired in a microplate reader (Synergy H1 version 2.09.1) and plotted using Prism 5.0. (Graph Pad, USA)

4.2.6. Quantum yield determination

The comparative fluorescence quantum yield (QY) of NS-CQDs was determined through the quinine sulfate (QY=54 % in 0.1 M H_2SO_4, λ_{ex}= 360 nm) as the reference. The detailed information is given in chapter 2 in section 2.6.1 (equation 2.1)

Table 4.1. Fluorescence QY determination of NS-CQDs with reference to quinine Sulfate at excitation wavelength 360 nm.

Sample	Integrated intensity at 360 nm	Absorbance at 360 nm	QY(%)
Quinine Sulphate (Reference)	96634914.21	0.098	54
NS-CQDs	66252364.10	0.095	37.8

4.2.7. Experimental methodology

The various advanced techniques were used for the characterization of blue fluorescent NS-CQDs. The morphology of NS-CQDs and size was investigated through the transmission electron microscopy (TEM) (Technai G2 20 TWIN), X-Ray diffraction (XRD) were measured by RigakuMiniflex 600 Desktop X-Ray diffraction System. The zeta potential was characterized through the Nano Zeta Sizer Malvern apparatus (4.0 mW laser), and time resolve fluorescence spectra was conducted by Edinburgh Instrument. Fourier transformed infrared spectroscopy (FT-IR) was conducted by using Perkin Elmer Spectrum 100 for the identification of functional groups. The chemical compositions and surface functional state were studied by X-ray photoelectron spectroscopy (XPS, AMICUS) and UV-visible absorbance elaboration was traced through a Thermo-Scientific, Evolution 201 spectrophotometer. The fluorescence emission spectra were carried out by HORIBA CANADA (PTI QM-400) fluorescence spectrophotometer.

4.3. Results and discussion

4.3.1. Characterizations

The NS-CQDs were prepared through the facile, low toxicity treatment process of CA, and TSC precursors at 180 ^{o}C for 5 hours, as displayed in **Scheme 4.1**.

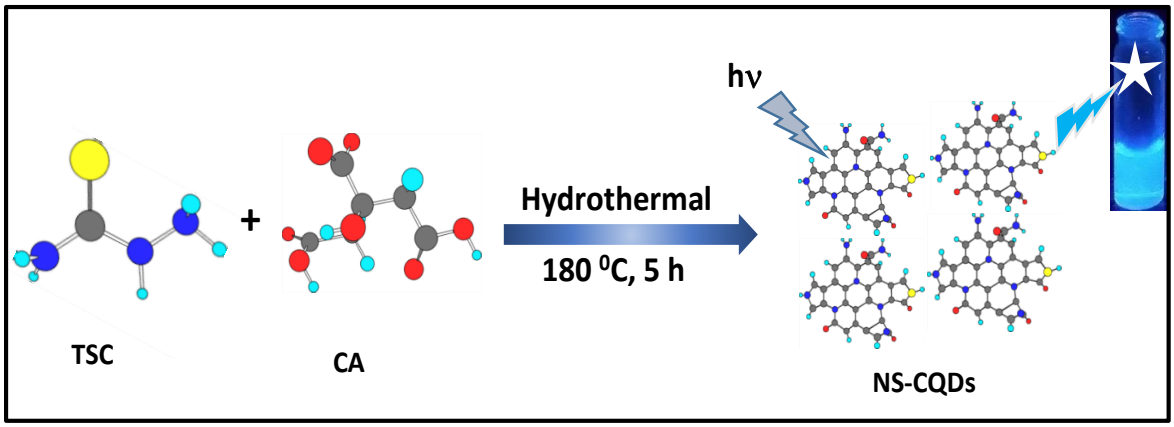

Scheme 4.1 Schematic illustration of the one-step hydrothermal synthesis of NS-CQDs via TSC and CA.

To probe the exact size and shape, the synthesized NS-CQDs were characterized through the TEM microscopy. As presented in **Figure 4.1a**, the typical TEM micrograph revealed that the as-prepared NS-CQDs have a spherical morphology and as well mono-dispersed from each other. The corresponding histogram obtained from the judged over 30 particles indicated that the size were distributed in the narrow range of 1.2 and 2.4 nm **(Figure 4.1b)**. The XRD spectrum of NS-CQDs exhibited a broad peak at $2\theta = 24.7^{o}$ along with the reflection of (002), which explores the amorphous structure of as-synthesized NS-CQDs, which is exhibited in **Figure 4.1c** [Bano *et al*. (2018)]. The attached functional groups on the NS-CQDs surface were employed by the FTIR analysis, as shown in **Figure 4.1d.** The typical peak at 3436 cm^{-1} is due to the –NH/–OH stretching vibration. The characteristic stretching peak at 3151 cm^{-1} represented the sp^2 –CH, whereas the peak at 2940 cm^{-1} for the sp^3 –CH band. The vibrational peak at 1725 cm^{-1} is accredited to the C=O stretching frequency while the peak at 1401 cm^{-1} assigned to the C=C stretching vibration. The stretching peak at 1211 cm^{-1} is due to the C–O/C–N/C–S. [Y Zhao et al. (2019), S Liao et al. (2018), Z Song et al. (2016)]. The FT-IR result reveals the presence of –NH, –OH, C=C, –

SH, and C=O functional groups on the NS-CQDs surface, which is responsible for the stability and solubility in an aqueous medium.

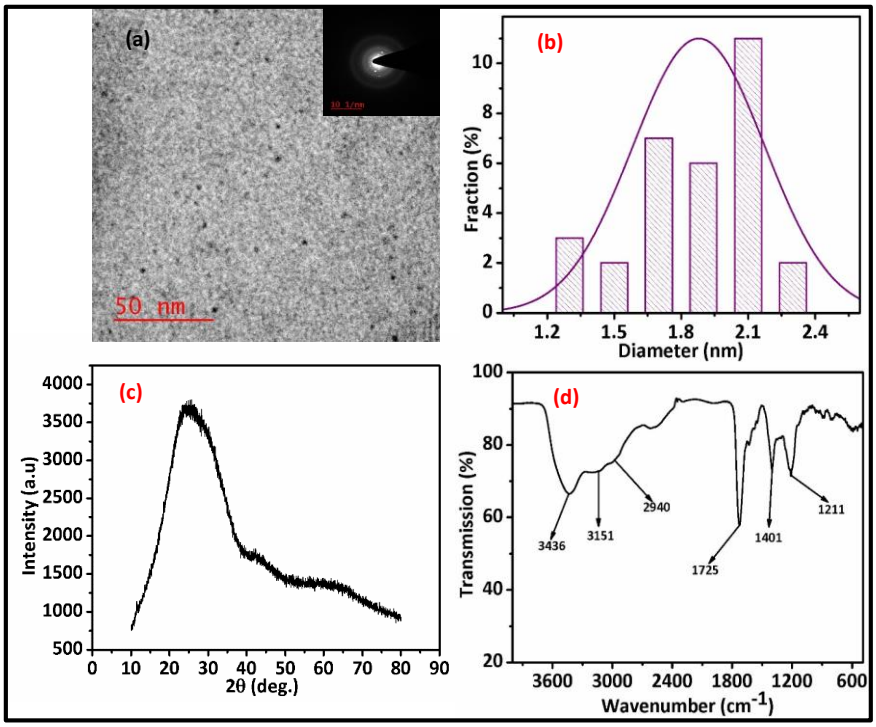

Figure 4.1 TEM micrograph of synthesized NS-CQDs with insect SAED image (a), Average size distribution histogram (b), P-XRD pattern, and (c) FT-IR spectrum of NS-CQDs.

The zeta potential of the as-prepared NS-CQDs is originated at 14.3 mV, as shown in (**Figure 4.2);** this result explored the presence of positively charged functional moieties on NS-CQDs surface, which stimulated the hydrophilicity, stability, and electronic properties NS-CQDs.

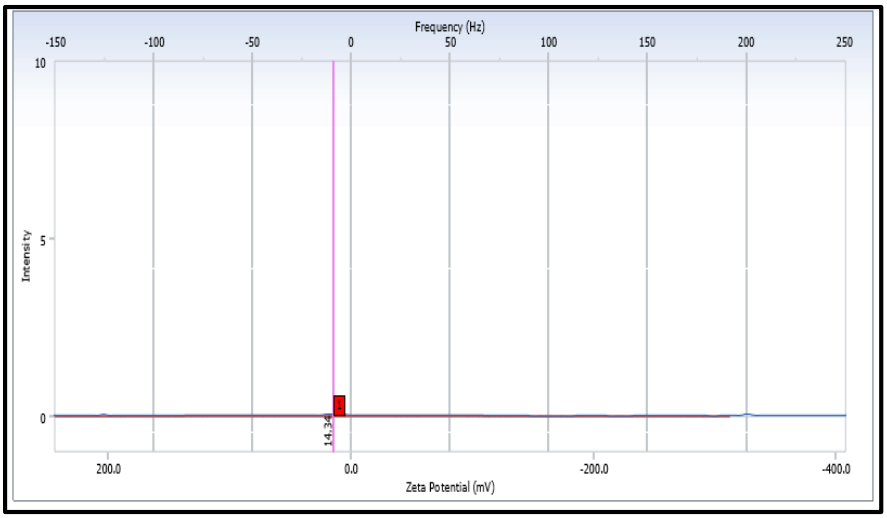

Figure 4.2 Zeta potential summary of as-synthesized NS-CQDs

To inspect the elemental arrangement and surface state, the XPS technique is used. As represented in (**Figure 4.3)**, the wide scan XPS spectrum displayed four peaks fixed at 286.6 eV, 399.4 eV, 531.8 eV, and 162.51 eV, which are credited to the C 1s, N 1s, O 1s, and S2p signals, respectively. This analysis established that C, N, O, and S were the main constituent of as-synthesized NS-CQDs.

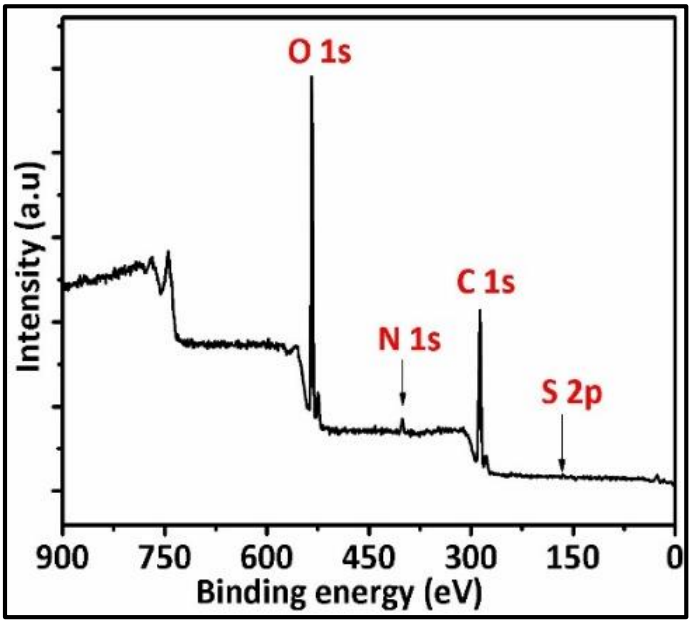

Figure 4.3 XPS wide scan spectrum of synthesized NS-CQDs.

Additionally, the high-resolution spectra of C1s exhibited five peaks around at 284.73 eV, 285.63 eV, 286.52 eV, 287.42 eV, and 288.50 eV, as shown in **Figure 4.4a,** which are due to the existence of C–C/C=C, C–N/C–O, C–S, C=O/C=N, and O=C–O^- groups, respectively. [C Zhu *et al.* (2012), S Chandra *et al*. (2019)] The N 1s spectrum in **Figure 4.4b** displayed the three peaks with the binding energies of 399.48 eV, 400.46 eV, and 401.47 eV, ascribed the presence of pyridinic (C–N–C), graphitic (N–C_3), and pyrrolic (N–H) moieties, respectively. Moreover, the high-resolution O 1s spectrum exhibited three distinct peaks at 532.62 eV, 533.55 eV, 534.43 eV **(Figure 4.4c),** which are due to the absorption of C=O, C–OH/S=O and COO^-, respectively. As for the S 2p spectrum, as shown in **Figure 4.4d,** the two types of chemical states with binding energies located at 163.2eV and 164.5 eV, which are responsible for the C–SH and C–S–C, respectively. [M Xue *et al.* (2015), Y Sun *et al.* (2015), D Bano *et al.* (2019)] Thus, XPS results consistent with the above aforementioned FT-IR data, which established the fruitful synthesis of NS-CQDs.

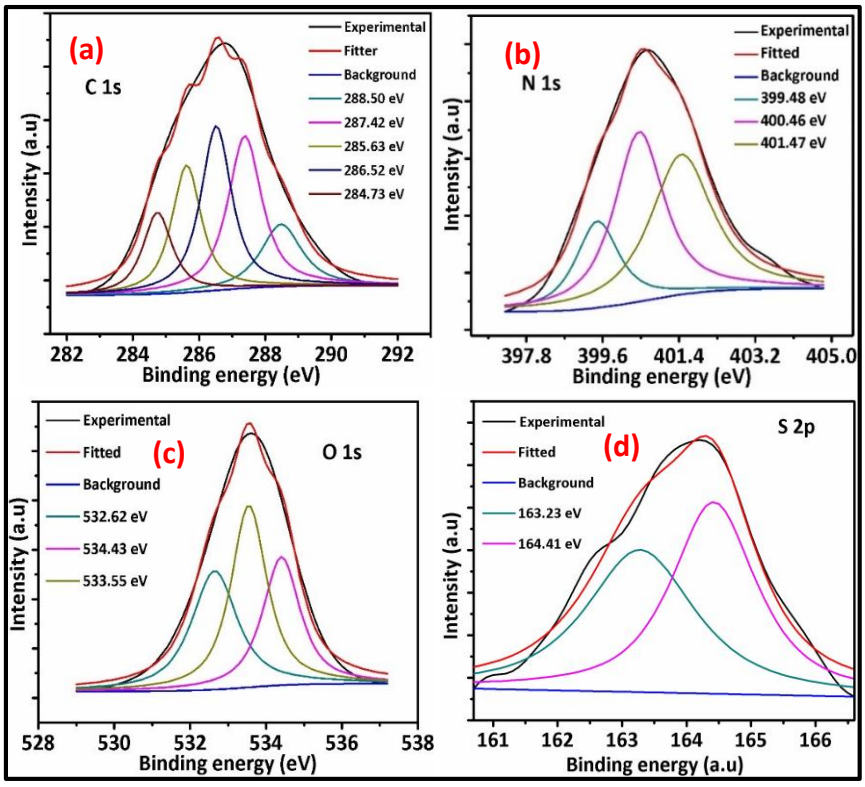

Figure 4.4 XPS spectra of (a) C1s (b) N1s (c), O1s spectra (d), and S2p NS-CQDs.

4.3.2. Optical Properties

To explore the photo-physical/optical properties of synthesized NS-CQDs, UV-visible absorbance, and fluorescence studies have been conducted. Here we observed that the UV-visible absorbance spectrum (Blackline) of NS-CQDs showed the two peaks at 295 nm and 366 nm, respectively. The absorption peak at 295 nm is ascribed to π -π* electron transition of C=C, whereas the other peak at 366 nm is validated the n-π* transition while the fluorescence spectrum (blue line) showed the emission peak at 435 nm at 360 nm excitation **(Figure 4.5a)**. [H Yang *et al.* (2019), D Bano *et al.* (2018)] Interestingly, the aqueous solution of NS-CQDs exhibiting blue color emissions under the UV-chamber at 365 nm excitation. As shown in **Figure 4.5b**, the blue color fluorescence of as-synthesized NS-CQDs is further confirmed by the CIE co-ordinate at (0.15, 0.07), which acquired from the

fluorescence emission data at 360 nm excitation. This outcome revealed the blue fluorescent under UV-light at 365 nm. The synthesized materials presented the excitation-dependent emission spectra (λ_{ex}: 240–400 nm) **(Figure 4.5c)**. Notably, the maximum emission is obtained at the 360 nm exciton, which is centered at 435 nm. Previous studies reported that the tuned fluorescence emission performance is due to the defected sites of surface-functionalized NS-CQDs. Furthermore, the high QY of NS-CQDs is found to be 37.8 % as compared to the quinine sulfate (QY = 54 %). The high QY triggered from the surface defect in a functionalized NS-CQDs encouraged by the electron-rich oxygen, nitrogen, and sulfur moieties, which are accountable for the ample of application such as sensing of toxic materials and other biological application. [Y Hu *et al.* (2017)] However, this yield was lower than reported in the literature. To gain deep insight, the stability of the prepared NS-CQDs was also investigated under the different physiological conditions such as the effects of pH, salt concentration, and exposure time. As shown in **Figure 4.5d**, the fluorescence emission spectra of NS-CQDs were acquired at different pH. It was found that the fluorescence intensity decreased with the increased pH value from 2 to 12, and the maximum emission intensity was obtained in highly acidic conditions at pH 2. It was further verified through the picture taken under UV-light at 365 nm excitation. The pH-dependent fluorescence emission was attributed to the different deprotonation degrees of functional moieties on NS-doped CQDs. [Y Song *et al.* (2014)] Therefore, optimum pH 2 was chosen for the sensing of PA.

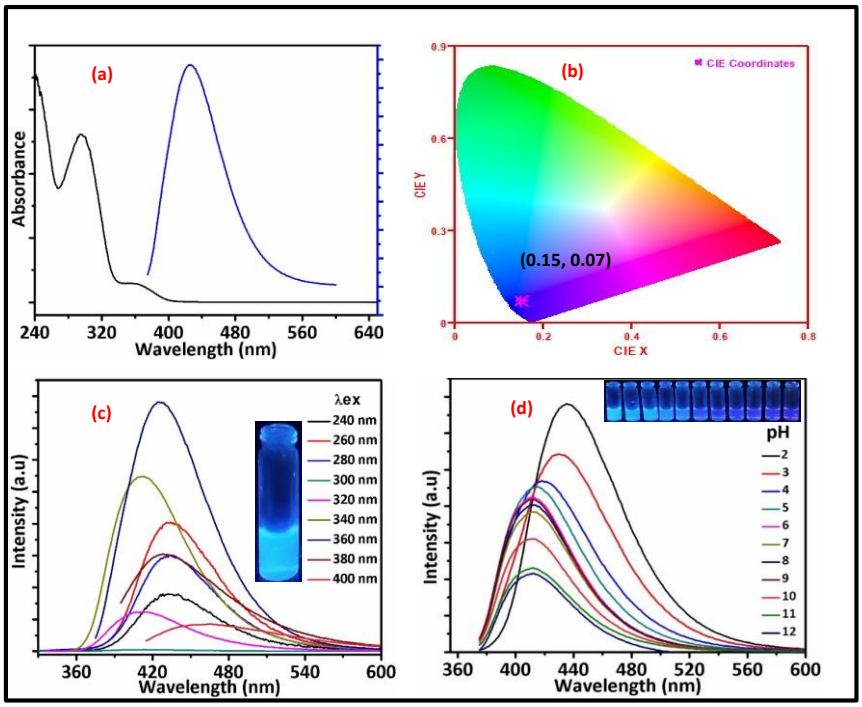

Figure 4.5 UV-visible absorption spectrum (black line) and Fluorescence spectrum (blue line) at the excitation of 360 nm (a), CIE Co-ordinates images shows the blue color of NS-CQDs (b) Fluorescence emission spectra show at the different excitation wavelength (240-400 nm) (c), represents the fluorescence intensity at different pH range from 2 to 12 (d).

The effect of ionic strength on NS-CQDs is probed with the addition of different NaCl concentrations ranges from 0 to 10 M. As indicated in **(Figure 4.6a),** the insignificant change in fluorescence emission confirmed that the as-prepared NS-CQDs did not aggregate even at a high salt concentration. These results suggested that the NS-CQDs have satisfactory salt-resistance and worthy properties for numerous applications in sensing and another pathological assay. Furthermore, the photo-stability of as-prepared NS-CQDs is examined by illuminating the sample for 5 months at 5 ^{o}C. Irrelevant change in the fluorescence **(Figure 4.6b)** ensured that the as-synthesized NS-CQDs have high photostability and durability.

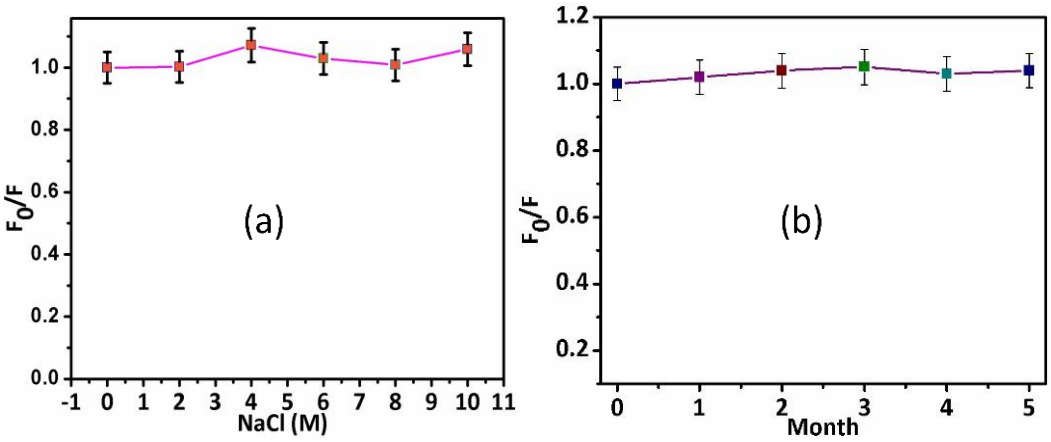

Figure 4.6 (a) Effect of fluorescence emission on adding different NaCl concentration. (b) Effect of fluorescence emission after 5 months of incubation at 5 ^{o}C.

4.3.3. Selectivity towards the detection of PA

The selectivity assay is the most significant parameter for the investigation of the sensing performance of the synthesized NS-CQDs. To know the selectivity for the PA detection, 50 μL of the prepared NS-CQDs were maintained in a 2 mL of Na-Ac buffer (0.2 M, pH 2). We have examined the selectively experiment toward the PA detection in a several nitro-containing aromatics and non-nitro aromatic compounds including phenol (Phe), nitrobenzene (NB), 2–chlorophenol (2–CP), 2,4–dinitrophenol (2,4–DNP), resorcinol (Res), iodobenzene (IB), bromobenzene (BB), 1,3–dinitrobenzene (1,3–DNB), 4–nitrophenol (4–NP), 2-nitrophenol (2–NP), and PA of concentration 100 μM under the optimum condition. As shown in **Figure 4.7a**, the high fluorescence quenching of NS-CQDs was obtained by the addition of PA compared to the addition of another nitro and non-nitro aromatics compounds. Moreover, to confirm the selectivity toward the PA detection, the fluorescence snapshot of NS-CQDs was taken under the UV chamber at 365 nm excitation wavelength **(inset Figure 4.7a)**. The above phenomenon could be based on the strong hydrogen bonding and π-π* interaction with electron-rich moieties on the surface of NS-

CQDs and the hydroxyl group of PA. Furthermore, the good selectivity towards PA in aqueous solution was further confirmed by the FRET mechanism.

The selectivity towards the detection of PA was also checked over a different metal ion counting Ag^{+}, Al^{3+}, Co^{2+}, As^{3+}, Cu^{2+}, Fe^{2+}, Fe^{3+}, Mn^{2+}, Na^{+}, Hg^{2+}, Pb^{2+}, Zn^{2+}, and Ni^{2+}. As represented in **Figure 4.7b**, an almost negligible effect was observed in the emission intensity of NS-CQDs by the addition of 100 μL of different metal ions (100 μM). This result indicates that the as-prepared NS-CQDs could still act as a probe even in the presence of numerous interfering metal ions.

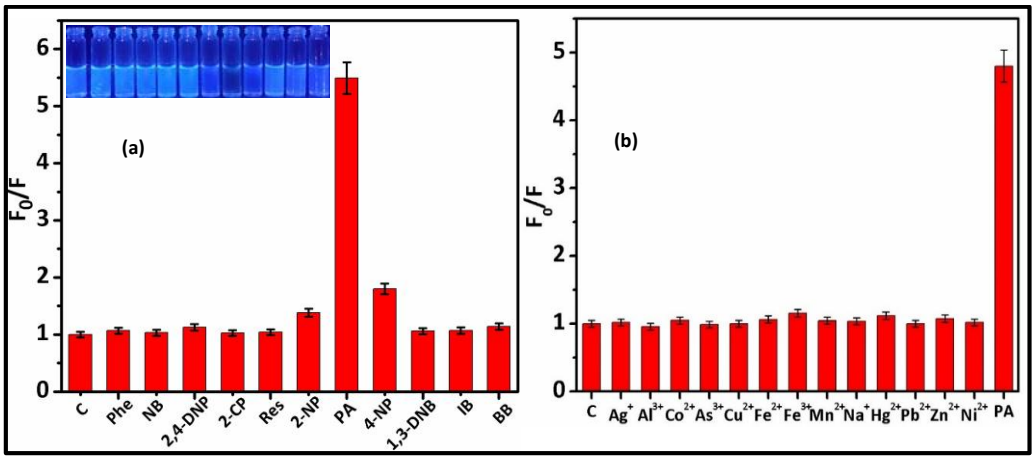

Figure 4.7 (a) Selectivity test of NS-CQDs for PA in the co-existence of different nitro and non-nitro explosives (concentration of PA and another explosive was 100 μM in 0.2 M sodium acetate buffer at pH 2), (b) Shows the interference study in different metal ions towards the PA detection, whereas, F_0 and F are the fluorescence emission intensity before and after the addition of various analytes.

4.3.4 Sensitivity assay

The sensing performance of as-synthesized fluorescent NS-CQDs for the PA detection was investigated under the optimum reaction condition with a varying concentration of PA. As shown in **Figure 4.8a**, the dependence fluorescence emission intensity of NS-CQDs was gradually decreased at 435 nm with the increased concentration of PA from 0 to 200 μM. As

shown in **Figure 4.8b**, an excellent linear relationship amid the $F_0/F-1$ and concentration of PA in the range of 0–3 μM is obtained with a good correlation coefficient (R^2 =0.996). The limit of detection (LOD) of PA was found to be 0.22 μM with a signal to noise ratio is 3 (S/N=3), which is very low compared to the earlier reported literatures (**Table 4.2).** In the same experiment, the Stern-Volmer quenching constant is calculated to be 0.03×10^6 mol^{-1}.L. The low detection limit and high quenching constant value indicated the good sensitivity of our synthesized nanoprobe. Thus our synthesized NS-CQDs is reliable for PA sensing.

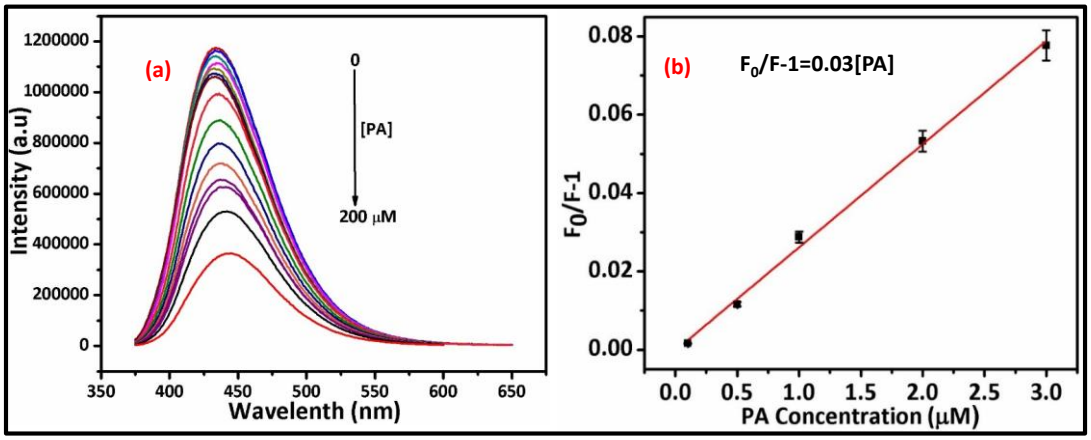

Figure 4.8 (a) Fluorescence emission intensity on increasing the concentration of PA from 0–200 μM **(b)** Shows the linear calibration graph between the concentration ranges of 0–3 μM.

Table 4.2. Comparison table for the PA detection with the earlier reported materials.

S.N	Material	Linear Range (μM)	LOD (μM)	Ref.
1	Graphene Oxide	-	0.55	[Dinda *et al*. (2014)]
2	Metal organic frameworks	0-50	2.5	[Shi *et al.* (2015)]
3	Conjugated Polymers	-	1	[Liu *et al*. (2014)]
4	CQDs	-	0.33	[Sk *et al.* (2014)]
5	CQDs	1-110	1.8	[Cheng *et al.* (2015)]
6	Amine capped CDs	-	1	[Niu *et al.* (2013)]

7	N-GQDs	1-60	0.30	[Lin *et al.* (2015)]
8	Covalent organic nanosheets	0.5-10	0.25	[Zhang *et al.* (2017)]
9	BNQDs	0.25-100	0.14	[Peng *et al*. (2018)]
10	CNPs	0.5-100	0.25	[Sun *et al.* (2016)]
11	NS-CQDs	0-3	0.22	Present work

4.3.5 Possible mechanism of PA sensing

The quenching mechanism for PA detection was further explored for its high selectivity and sensitivity. As shown in **Figure 4.9a**, the strong spectral overlapping occurred among the absorption spectrum of PA and emission as well as the excitation spectrum of NS-CQDs. As the PA possesses a broad absorption band of 280 to 490 nm, the excitation and emission spectrum of NS-CQDs centered at 360 nm and 435 nm. This explores the possibility of fluorescence resonance electron transfer (FRET) or the Inner Filter Effect (IFE). Subsequently, the addition of PA lowered the average fluorescence lifetime 8.14 ns from 9.40 ns than that of NS-CQDs, as shown in **Figure 4.9b**; the additional data related to three exponential fittings of lifetime spectra are given in the **(Table 4.3)**.

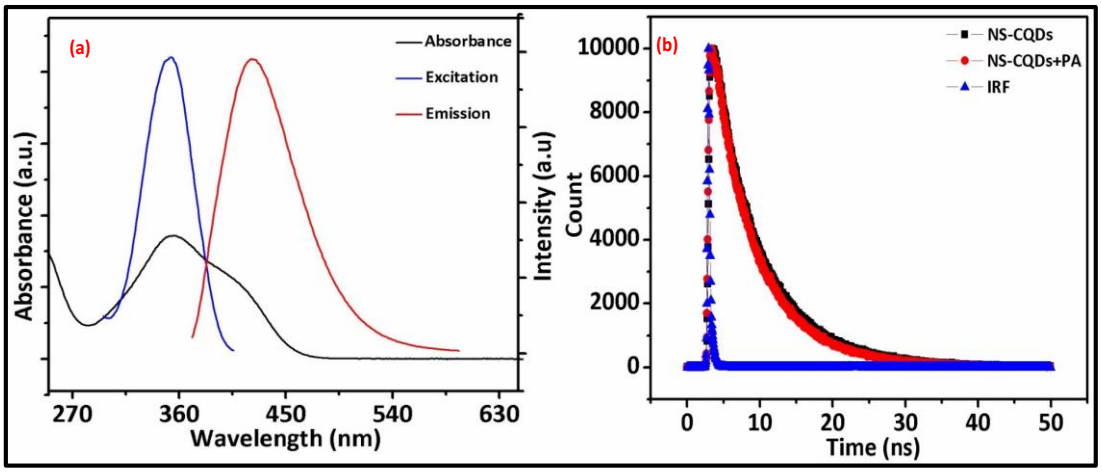

Figure 4.9 (a) Represents the overlapping of the absorption spectrum of PA with the emission and excitation of NS-CQDs, (b) shows the time resolve fluorescence spectra of NS-CQDs with and without PA.

Table 4.3. Fitting data of fluorescence lifetimes for the NS-CQDs and the NS-CQDs+PA hybrid.

Sample	chi-square (χ^2)	Different lifetime (ns)	Weight (%)	Average lifetime (ns)
NS-CQDs	1.1564	τ_1=0.68 τ_2=4.14 τ_3=12.76	20.78 50.65 28.57	9.40
NS-CQDs+PA	1.216	τ_1=0.39 τ_2=2.16 τ_3=9.76	15.12 45.36 39.52	8.14

The lifetime reduction demonstrates the interaction between the electron-rich nitrogen atom on the surface of NS-CQDs and the electron-deficient nitro-group of PA. These results show that FRET is the dominant mechanism between FRET and IFE, which is supported by the previous literature. Further, the Zeta potential of NS-CQDs reduced to 2.56 mV from 14.34 mV in the presence of 100 μL of PA (100 μM) which confirmed that PA is absorbed by the synthesized NS-CQDs and form a non-fluorescent complex through the strong electrostatic interaction amid the NS-CQDs and PA **(Figure 4.2 and Figure 4.10).** [D Bano

et al. (2019)] Thus, the outstanding selectivity towards the PA detection is based on the FRET from NS-CQDs to PA and the formation of the non-fluorescent complex between the NS-CQDs and PA.

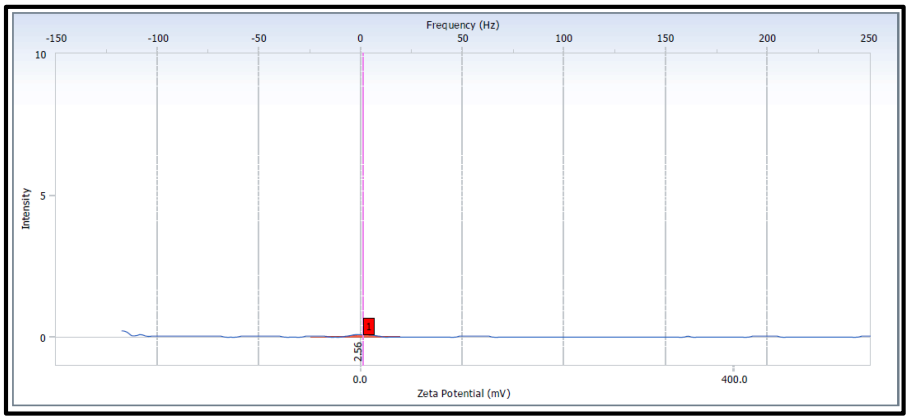

Figure 4.10 Zeta potential of NS-CQDs after the addition of PA

4.3.6 Biocompatibility & Cell Viability

The compatibility of the quantum dots in living cells is critical for its utilization in biological systems. Biocompatibility and minimal required concentration for conferring fluorescence were evaluated by incubating HeLa cells with varying concentrations of the NS-CQDs. Detectable levels of fluorescence were observed in the cells exposed to 6 mg/mL or higher concentrations of NS-CQDs (**Figure 4.11a**). The NS-CQDs were found to be completely non-toxic to the cells in the treated concentration range (**Figure 4.11b**). Therefore, our results suggest that the NS-CQDs are biologically compatible and non-toxic to be employed for diagnostics purposes.

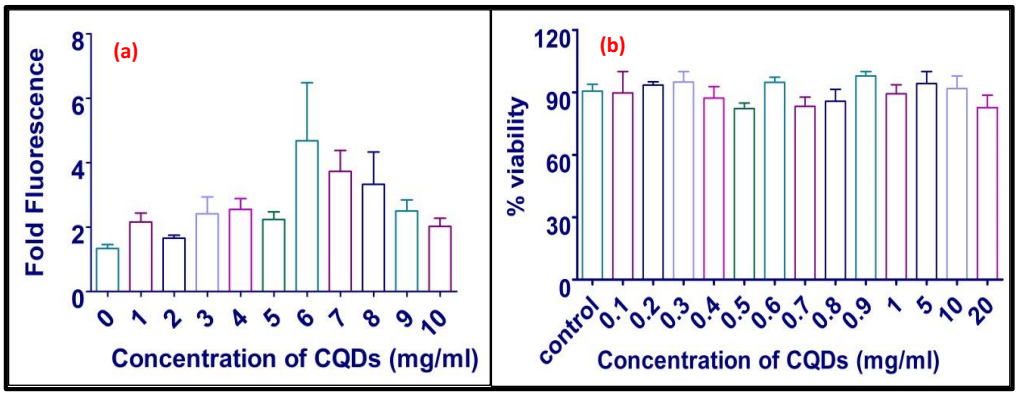

Figure 4.11 (a) The HeLa cells incubated with increasing concentrations of the NS-CQDs were quantified for fluorescence intensity as a measure of NS-CQDs uptake and staining. The intracellular fluorescence intensity was depicted as fold fluorescence in the form of a bar graph, (b) The HeLa cells were exposed to a variable concentration of the NS-CQDs, and the degree of cellular viability was estimated using MTT assay. The detected absorbance was represented as percent cell viability.

4.3.7 Picric acid sensing in living cells

PA with its several military and industrial applications has a potential negative impact on both humans and wildlife with 2 milligrams per kilogram per day (mg/kg/day) as mammalian no observed adverse effect level (NOAEL) based Toxicity Reference Value (TRV), and 10 mg/kg/day as the lowest observed adverse effect level (LOAEL) based TRV. [RM Hebert *et al.* (2015)] This low threshold level of PA for the onset of toxicological effects calls for the detection of PA at lower concentrations for environmental protection as well as national security. Selective sensing of PA was demonstrated in cells treated with minimum 8 mg/mL NS-CQDs which showed immediate quenching of fluorescence when treated with PA concentration as low as 0.05 mg/ml (**Figure 4.12**). This indicates the very high sensitivity of the NS-CQDs for PA detection and equips it with the potential advantage for use in intracellular detection of this toxin.

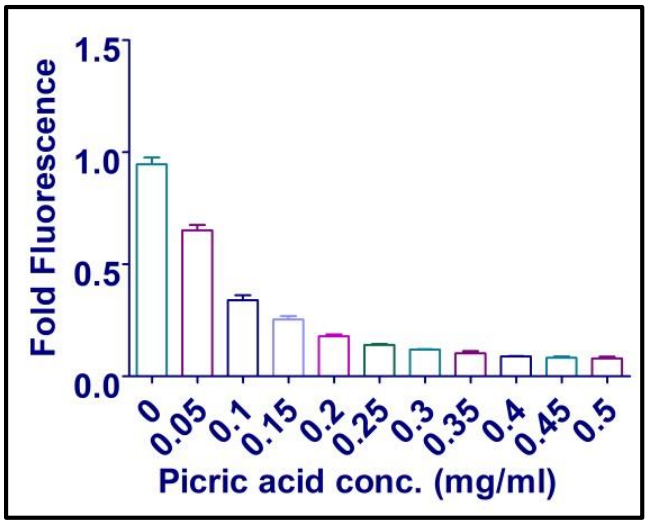

Figure 4.12 Graph depicting decreasing fold fluorescence in pre-treated cells when subjected to increasing concentration of PA.

4.4. Detection of PA in a real environmental sample

To **Figure** out the practical feasibility of our proposed analytical method, the as-prepared NS-CQDs sensor was used for the detection of PA in a real aqueous solution. The real sample of Pond water was collected from the Indian Institute of Technology IIT (BHU) Varanasi, India. The experiment was performed with the spike of water samples in the different known solutions of PA. **(Table 4.4)** shown the sample recovery range varying from 99.2-103.6 %, and the relative standard deviation (RSD) of the three times investigation for each sample is less than 5. Hence, this analysis assay confirmed the excellent accuracy, recovery, and good reliability. Consequently, this sensor has a potential application for the determination of PA in practical samples.

Table 4.4. Standard recovery experiment after spiking with PA of different concentration in the pond water sample

Sample	**Spiked PA (μM)**	**Found PA (μM)**	**Recovery (%)**	**RSD (%)**
Pond water	0	0	-	1.76
	10	10.36	103.6	1.48
	20	19.84	99.2	1.63

4.5. Conclusion

In precise, we have efficaciously synthesized environmentally friendly nitrogen sulfur-doped fluorescent carbon quantum dots (NS-CQDs) from the precursors CA and TSC. The as-prepared NS-CQDs shown the excitation-dependent tuned emission in the range of 240–400 nm with the high fluorescence QY 37.8 %. Moreover, the synthesized NS-CQDs served as a sensitive nano-probe for the detection of PA with high selectivity and sensitivity along with the LOD 0.22 μM in the obtained linear range of 0–3 μM of PA concentrations. The NS-CQDs possess relatively high biocompatibility and can stain the cells without any significant toxicity at biological concentrations. Its ability to detect PA in nano-grams levels extends its usage for the detection of very low concentrations of the toxin in biological and environmental systems. Apart from this, the proposed sensing system had also applied to the pond water as an environmental sample to quantify the PA concentration, which demonstrated the potential applicability of our system toward PA detection.